Research Square

Preprints are preliminary reports that have not undergone peer review.
They should not be considered conclusive, used to inform clinical practice,
or referenced by the media as validated information.

Parametric overturning-stability assessment of a compact construction transport vehicle equipped with a crane boom

Yunfeng Dai

lyzzjdx12@163.com

State Grid Yancheng Power Supply Company

Feng Zhao

State Grid Yancheng Power Supply Company

Hongmei Cui

State Grid Yancheng Power Supply Company

Yihua Wang

State Grid Yancheng Power Supply Company

Yubing Wang

State Grid Yancheng Power Supply Company

Article

Keywords: mobile crane, construction transport vehicle, overturning stability, support polygon, wind load, slope, uncertainty analysis

Posted Date: August 28th, 2026

DOI: https://doi.org/10.21203/rs.3.rs-10653686/v1

License: This work is licensed under a Creative Commons Attribution 4.0 International License.
Read Full License

Additional Declarations: No competing interests reported.

Version of Record: A version of this preprint was published at Scientific Reports on November 17th, 2026. See the published version at https://doi.org/10.1038/s41598-026-80331-5.

Parametric overturning-stability assessment of a compact construction transport vehicle equipped with a crane boom

Yunfeng Dai[1]*, Feng Zhao[1], Hongmei Cui[1], Yihua Wang[1] , Yubing Wang[1]

[1]State Grid Yancheng Power Supply Company, Yancheng 224000, Jiangsu, China

**Correspondence: Yunfeng Dai ,lyzzjdx12@163.com*

Abstract

Compact transport vehicles are increasingly fitted with articulated or telescopic crane booms to solve last-kilometre material-handling problems at transmission-line construction sites. The modification changes a low-speed carrier into a mobile lifting system whose stability depends simultaneously on payload, boom reach and azimuth, support geometry, road slope, transient acceleration and wind. The four rated configurations—200 kg at 3.60 m, 310 kg at 2.70 m, 450 kg at 1.95 m and 800 kg at 1.13 m—were evaluated over 360° boom rotation, slopes from 0° to 8.5°, wind speeds from 0 to 20 m s−1 and central deck masses from 0 to 1500 kg. A fixed-seed Monte Carlo analysis propagated uncertainty in deck mass, slope, wind, boom acceleration, lifting coefficient and centre-of-gravity location through 10,000 model evaluations per configuration. The results show that rated load alone is not a sufficient safety descriptor. With a 1000 kg central deck mass, 3° outward slope and 15.5 m s−1 wind, the minimum dimensionless stability index ranged from −0.133 to 0.111 across the four configurations; the narrow longitudinal support dimension governed the worst azimuths. Increasing central deck mass improved the index, but the two longest-reach configurations still required azimuth restrictions or a larger support polygon to maintain a 0.10 reserve. The model-derived results are not hardware measurements; they define testable design hypotheses, an auditable pre-test screening method and explicit limits for subsequent prototype validation.

Keywords: mobile crane; construction transport vehicle; overturning stability; support polygon; wind load; slope; uncertainty analysis

Introduction

Construction of overhead transmission lines frequently crosses narrow village roads, unpaved access tracks and temporary work areas whose bearing capacity and cross-slope are less controlled than those of an industrial yard. Full-size trucks or truck cranes may be unable to reach the foundation or tower-assembly location, so compact tyre- or track-based carriers are used to move sand, tower members, tools and cable-handling equipment. Adding a small crane boom reduces repeated trans-shipment and manual handling, but it also transfers payload weight and dynamic forces far outside the short chassis wheelbase. The resulting machine is neither an ordinary low-speed carrier nor a conventional certified mobile crane. Its safety therefore cannot be inferred from nominal payload capacity alone.

Recent crane research increasingly treats stability as a configuration-dependent computational problem. Computer-aided rotary-crane assessment has demonstrated the value of evaluating the instantaneous support condition rather than relying on a single catalogue capacity [1]. Wind-aware crane selection similarly shows that environmental loading and geometry must be evaluated together [2]. For mobile manipulators operating on rough terrain, stability-constrained planning incorporates terrain inclination and a support-based stability measure directly into motion generation [3], while analytical wheel-load solutions show that loss of positive support reaction is a physically interpretable tipping precursor [4]. These developments motivate a transparent edge-reaction or edge-moment formulation for compact construction carriers.

Boom configuration is especially important because equal end-effector speeds or equal lifted masses do not create equal overturning moments. Configuration selection for modular mobile manipulators has shown that the wrench transmitted to the base changes substantially with arm posture [5]. Positioning studies of mobile-crane loading systems also emphasise the coupled influence of sequential joint motion, structural deformation

and control accuracy [6]. At a field site, these geometric effects interact with imperfect platform levelling. A support-vector-machine method for all-terrain cranes illustrates the practical importance of identifying road level [7], and recent crane-platform control research focuses on coordinated outrigger levelling precisely because small attitude errors redistribute support forces [8].

Wind and ground inclination are not secondary corrections. Numerical and analytical work on crane overturning demonstrates that critical wind speed changes with crane orientation and payload configuration [9]. Wind-induced load sway can further amplify a nominally static load case [10]. Digital-twin lift planning has therefore begun to combine crane position, capacity and spatial constraints before execution [11]. Parallel evidence from agricultural and off-road vehicles is relevant because compact construction carriers share a narrow track, elevated centre of gravity and compliant chassis. A recent review identifies centre-of-gravity height, slope, speed, tire-ground interaction and active control as recurring rollover determinants [12]. Chassis torsional flexibility can change the predicted rollover threshold [13], and multidimensional vehicle studies show that speed, height and steering inputs interact nonlinearly [14]. Pavement roughness and differential settlement also reduce both rollover and skidding margins [15].

Crane design standards enumerate self-weight, lifting impact, sudden unloading, travel impact, translational inertia, slewing and luffing inertia, operating wind and non-operating wind. For a compact 2.000 m × 1.100 m carrier, however, these actions must be integrated with a configuration-dependent support polygon before they can define a measurable stability margin. Three methodological issues are therefore central: the unloaded mass must be decomposed consistently among the chassis, boom and auxiliary systems; every vertical and horizontal action must be resolved about each candidate tipping edge; and uncertainty must be propagated so that influential assumptions can be distinguished from negligible ones.

Accordingly, this study develops a reproducible parameter study in which the 500 kg chassis is one component of a 1000 kg unloaded vehicle that also includes the 200 kg moving boom assembly and 300 kg of drive, battery, hydraulic and structural components. A rectangular support polygon represents the wheel centre lines in travel mode and the deployed outrigger lines in lifting mode. For every candidate state, the vertical and horizontal loads are projected onto the four possible tipping edges and the minimum signed edge moment is normalised to obtain a dimensionless stability index. Deterministic sweeps, a continuous load–radius envelope and fixed-seed uncertainty propagation answer three questions: which boom directions govern stability; how slope, wind and deck mass change the margin; and which uncertain parameters most strongly affect the result.

Methods

Study design and evidence boundary

The study combines a deterministic mechanics model with fixed-seed uncertainty propagation. No human, animal or field measurements were collected. Geometry, rated payloads and coefficients are defined in Tables 1–6, while unmeasured force heights and component coordinates are stated explicitly as modelling assumptions. The workflow in Fig. 6 begins with parameter definition and mass harmonisation, proceeds through load and support models, and ends with scenario screening, sensitivity analysis and an engineering operating envelope. Computed values are reported as numerical screening results rather than physical measurements.

The analysis considered two support modes. Travel mode used the wheel centre-line rectangle, 1.130 m longitudinally by 0.990 m laterally. Lifting mode used the deployed outrigger rectangle, 1.130 m longitudinally by 1.604 m laterally. The rear hydraulic outriggers enlarge lateral support without increasing the longitudinal span. Because a rectangular support polygon has four possible tipping edges, the governing edge changes with boom azimuth. A state was classified as statically admissible when every calculated edge moment was non-negative. For design screening, a reserve criterion $SI \geq 0.10$ was also applied; this threshold is a study assumption, not a claim that a particular code mandates the value.

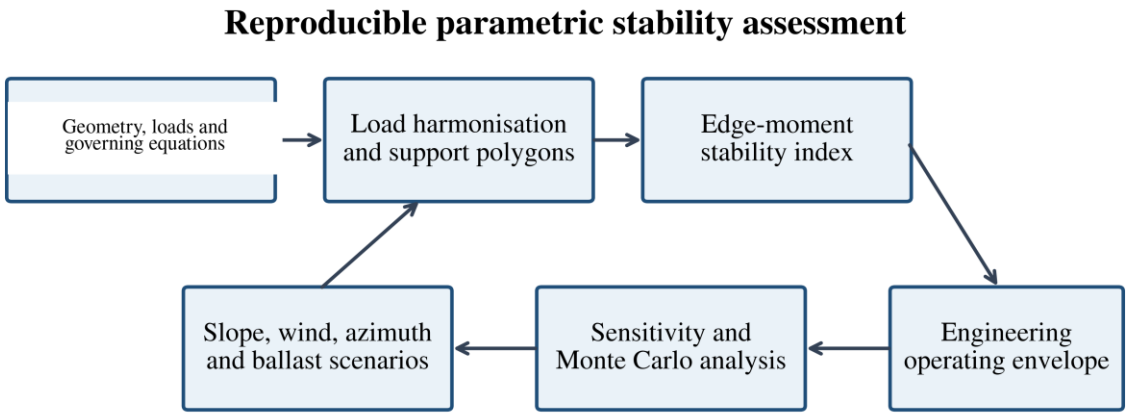


Figure 6. Reproducible workflow from parameter definition to support-edge stability results, sensitivity analysis and the engineering operating envelope. The outputs are computational predictions rather than hardware measurements.

Vehicle and crane parameters

The vehicle is 2.000 m long, 1.100 m wide and 0.670 m high, with a 1.130 m wheelbase and 0.990 m track. Table 1 specifies a 500 kg chassis, a maximum carrying mass of 1500 kg, a maximum speed of 10 km h−1, a 15% nominal gradeability and an unloaded centre of gravity 0.782 m from the front axle and 0.796 m above ground. A reported lateral coordinate of 0.570 m from the side of the 1.100 m vehicle is interpreted as a 0.020 m offset from the geometric mid-plane; treating it as a centreline coordinate would place the centre of gravity outside the vehicle envelope.

The unloaded analysis mass is defined as 1000 kg: 500 kg for the chassis, 200 kg for the moving boom assembly and 300 kg for propulsion, batteries, hydraulic equipment, mounting frame and bodywork. The moving boom is separated from an 800 kg fixed remainder when its orientation is varied. The fixed-remainder coordinate is selected so that the combined unloaded centre of gravity remains 0.782 m from the front axle for the retracted 800 kg configuration. Central deck cargo or ballast is varied independently from 0 to the 1500 kg carrying limit.

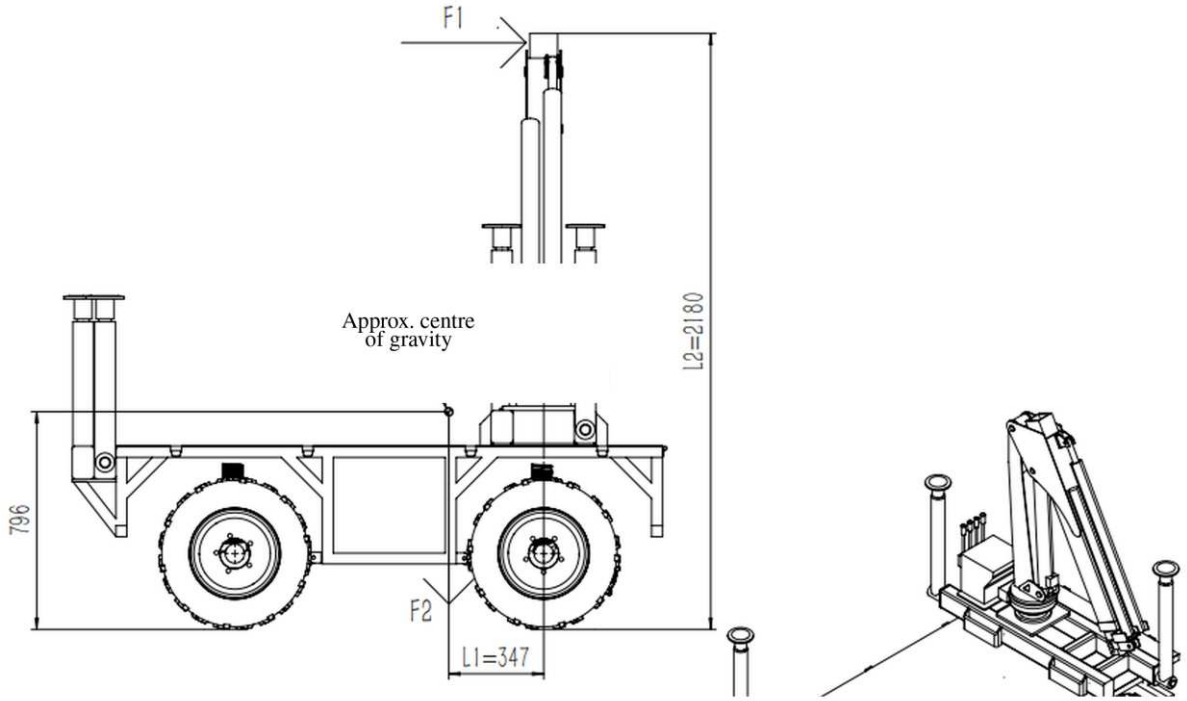
Table 1. Chassis parameters and modelling definitions.

Parameter	Parameter value	Model interpretation
Overall dimensions	2000 × 1100 × 670 mm	Specified vehicle envelope
Wheelbase / track	1130 / 990 mm	Travel support polygon
Chassis mass	500 kg	Part of 1000 kg unloaded analysis mass
Maximum carrying mass	1500 kg	Upper bound for central deck mass
Maximum speed	10 km h−1	Not used during stationary lifting
Maximum gradeability	15% (approximately 8.5°)	Upper slope sweep
Turning radius	5 m	Context only
Unloaded centre of gravity	782 mm from front axle; 796 mm high	20 mm lateral offset inferred from geometry

Table 2. Rated payload–reach configurations evaluated in the stability analysis.

Rated case	Payload	Horizontal reach	Boom centre-of-mass radius	Projected boom area
I	200 kg	3.60 m	1.807 m	1.341 m²

Rated case	Payload	Horizontal reach	Boom centre-of-mass radius	Projected boom area
II	310 kg	2.70 m	1.6765 m	1.341 m²
III	450 kg	1.95 m	1.4345 m	1.341 m²
IV	800 kg	1.13 m	1.009 m	0.900 m²



Notes: 1 F2: vehicle self-weight; F1: wind load.
2 L1 and L2 are lever arms. 3 The front-wheel centreline is the tipping line.
4 Conservatively, the wind load is applied at the boom tip.

Figure 1. Vehicle, crane-boom and force-arm drawing

Load equations and coefficient normalisation

A consistent SI formulation is used throughout the load model. Gravitational acceleration is set to 9.81 m s−2, and every mass is converted to force before moment calculation. The unloaded self-weight and four rated payload weights are given by Eqs. (1)–(5), which maintain a strict distinction between mass in kilograms and force in newtons.

$$P_G = m_v g = 1000 \times 9.81 = 9810\ \text{N} \tag{1}$$

$$P_{Q,1} = m_{Q,1} g = 200 \times 9.81 = 1962\ \text{N} \tag{2}$$

$$P_{Q,2} = m_{Q,2} g = 310 \times 9.81 = 3041.1\ \text{N} \tag{3}$$

$$P_{Q,3} = m_{Q,3} g = 450 \times 9.81 = 4414.5\ \text{N} \tag{4}$$

$$P_{Q,4} = m_{Q,4} g = 800 \times 9.81 = 7848 \text{ N} \tag{5}$$

The self-weight vibration coefficient is φ1 = 1 ± α with α = 0.10; the upper value 1.10 is used for conservative screening. The lifting dynamic coefficient follows the HC2 selection, with minimum coefficient 1.10, slope coefficient β2 = 0.34 and steady lifting speed 0.30 m s−1. Equations (6)–(12) define the corresponding dynamic loads, while Fig. 2 and Table 3 summarise the coefficient relationship and four hoisting-condition classes.

$$P_{G,d} = \phi_1 P_G = 1.10 \times 9810 = 10791 \text{ N} \tag{6}$$

$$\phi_2 = \phi_{2,\min} + \beta_2 v_h \tag{7}$$

$$\phi_2 = 1.10 + 0.34 \times 0.30 = 1.202 \tag{8}$$

$$P_{Q,d,1} = \phi_2 P_{Q,1} = 2358.3 \text{ N} \tag{9}$$

$$P_{Q,d,2} = \phi_2 P_{Q,2} = 3655.4 \text{ N} \tag{10}$$

$$P_{Q,d,3} = \phi_2 P_{Q,3} = 5306.2 \text{ N} \tag{11}$$

$$P_{Q,d,4} = \phi_2 P_{Q,4} = 9433.3 \text{ N} \tag{12}$$

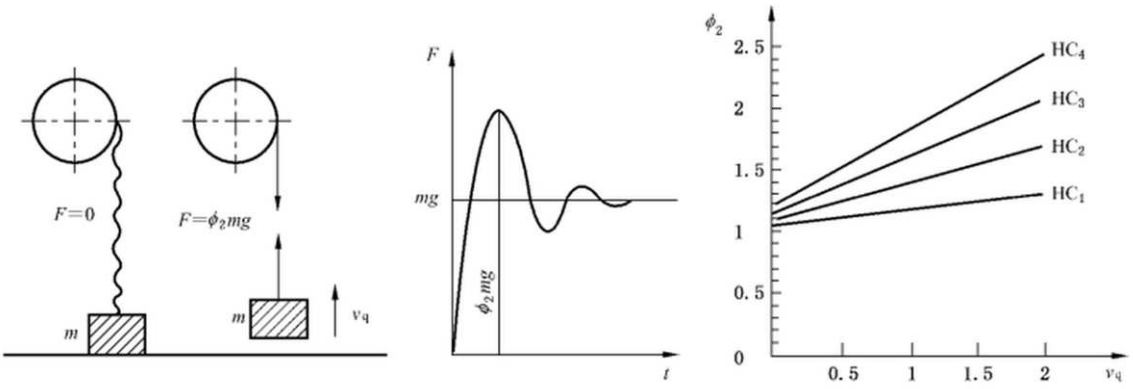


Figure 2. Dynamic coefficient phi2

Figure 2. Relationship between lifting speed and the lifting-dynamic coefficient for hoisting classes HC1–HC4.

Table 3. Dynamic-coefficient parameters β₂ and φ₂,min for the four hoisting classes.

Hoisting class	β₂	φ₂,min	Interpretation
HC1	0.17	1.05	Smooth lift-off
HC2	0.34	1.10	Slight impact; selected
HC3	0.51	1.15	Moderate impact
HC4	0.68	1.20	High impact

Sudden unloading is represented through φ3 in Eq. (13). The coefficient depends on the released fraction Δm/m and on whether unloading is slow (β3 = 0.5) or rapid (β3 = 1.0). Because no specific release event is included in the baseline scenarios, this term is activated only when the handling process can drop or release part of a suspended mass.

$$\phi_3 = 1 - \frac{\Delta m}{m}(1 + \beta_3) \tag{13}$$

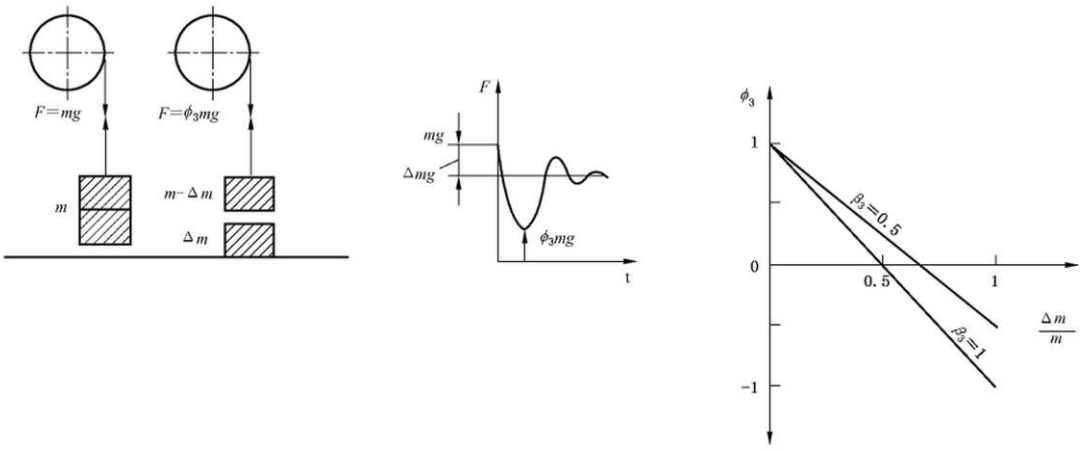


Figure 3. Unloading coefficient phi3

Figure 3. Sudden-unloading coefficient as a function of released mass fraction.

Travel impact and horizontal translational inertia are evaluated separately from stationary lifting. For travel speed above 0.4 m s−1, φ4 = 1.30. Equations (14) and (15) give the vertical travel-impact loads for an unloaded 1000 kg vehicle and a vehicle carrying 1000 kg on the deck. With reference acceleration 0.39 m s−2 and amplification φ5 = 2.0, Eqs. (16) and (17) give the horizontal inertial forces. Combining these travel cases with stationary outrigger-supported lifting would imply physically incompatible operating states.

$$P_{R,0} = \phi_4 m_v g = 1.30 \times 1000 \times 9.81 = 12753 \text{ N} \tag{14}$$

$$P_{R,\max} = \phi_4 (m_v + m_T) g = 25506 \text{ N} \quad (m_T = 1000 \text{ kg}) \tag{15}$$

$$F_{H,0} = \phi_5 m_v a = 2.0 \times 1000 \times 0.39 = 780 \text{ N} \tag{16}$$

$$F_{H,\max} = \phi_5 (m_v + m_T) a = 1560 \text{ N} \tag{17}$$

Table 4. Reference acceleration values for travel dynamics.

Target speed	Long-distance acceleration	Normal acceleration	High acceleration
4.00 m s^{-1}	–	0.50 m s^{-2}	0.67 m s^{-2}
3.15	–	0.44	0.58
2.50	0.220	0.39	0.52
2.00	0.190	0.35	0.47
1.60	0.150	0.32	0.43
1.00	0.120	0.25	0.33

Target speed	Long-distance acceleration	Normal acceleration	High acceleration
0.63	0.098	0.19	–
0.40	0.078	0.16	–
0.25	0.064	–	–

Boom-slewing and luffing inertia is represented by an acceleration a_s = 0.20 m s−2 applied to the 200 kg boom assembly and the corresponding payload. Equations (18)–(21) define the four inertial-force cases. Figure 4 consolidates the four rated configurations without altering their dimensions or centre-of-mass locations.

$$F_{s,1} = (m_b + m_{Q,1})a_s = (200 + 200) \times 0.2 = 80 \text{ N} \tag{18}$$

$$F_{s,2} = (200 + 310) \times 0.2 = 102 \text{ N} \tag{19}$$

$$F_{s,3} = (200 + 450) \times 0.2 = 130 \text{ N} \tag{20}$$

$$F_{s,4} = (200 + 800) \times 0.2 = 200 \text{ N} \tag{21}$$

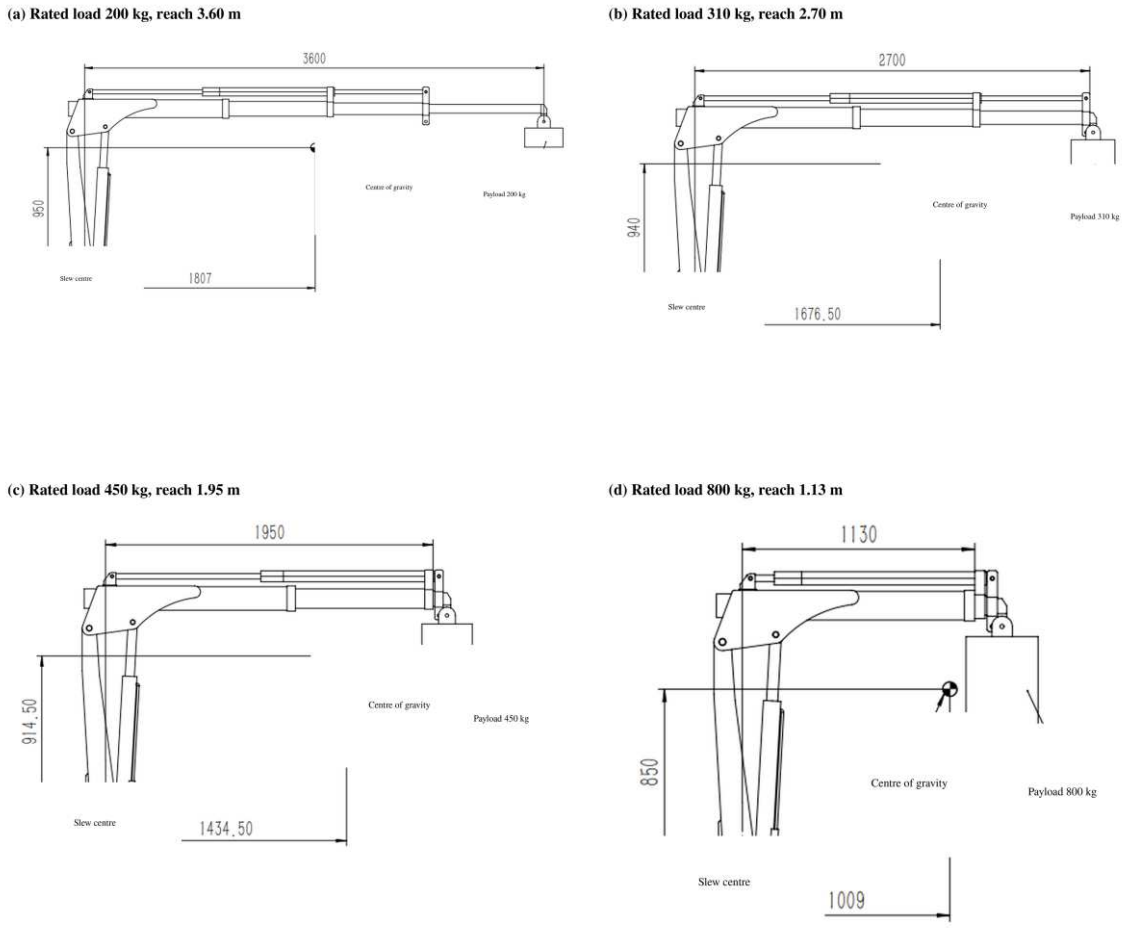


Figure 4. Rated boom configurations: (a) 200 kg at 3.60 m, (b) 310 kg at 2.70 m, (c) 450 kg at 1.95 m and (d) 800 kg at 1.13 m.

Operating and non-operating wind loads are defined in Eqs. (22)–(24). The aerodynamic model uses drag coefficient C = 1.3, boom projected areas of 0.900 m² when retracted and 1.341 m² when fully extended, and a maximum payload projected area A_Q = 0.50 m². Wind pressures of 150 N m−2 for general inland operation and 500 N m−2 for Beaufort-force-8 conditions are evaluated. In the parametric figures, pressure is calculated from wind speed using Eq. (29), giving approximately 147 N m−2 at 15.5 m s−1 and agreeing closely with the 150 N m−2 operating value.

$$F_W = CpA \tag{22}$$

$$F_{WQ} = 1.2pA_Q \tag{23}$$

$$F_{W,III} = CK_h p_{III} A \tag{24}$$

Table 5. Working and non-operating wind-pressure values used in the analysis.

Operating region / condition	pI	pII	Corresponding speed
General inland operation	0.6pII	150 N m^{-2}	15.5 m s^{-1}
Coastal / island operation	0.6pII	250 N m^{-2}	20.0 m s^{-1}
Operation permitted in force-8 wind	–	500 N m^{-2}	28.3 m s^{-1}

Table 6. Load-combination families A, B and C used for travel, lifting and exceptional conditions.

Combination	Parameter definition	Use in analysis
A1–A4	Normal operation without working wind	Deterministic zero-wind comparisons
B1–B5	Corresponding normal cases with working wind; B5 includes slope	Baseline coupled slope–wind screens
C1–C9	Special lifting, non-operating wind, proof load, collision or failure cases	Discussed but not numerically combined without event data

G.1.3.3.1 Permitted combinations (see Fig. G.3):
- Hoisting (H) and slewing (S)
- Hoisting (H) and luffing (L)
- Hoisting (H) and telescoping (Te)
- Slewing (S) and luffing (L)
- Slewing (S) and telescoping (Te)
- Telescoping (Te) and luffing (L)
- Travel with load (T)

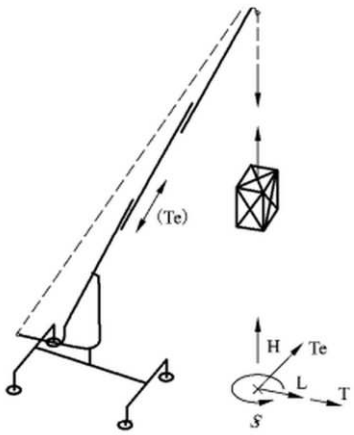


Figure G.3. Wheeled/mobile crane with a telescopic boom

Figure 5. Permissible combinations of simultaneous crane movements.

Support-edge stability formulation

The combined centre of gravity is calculated with Eq. (25). For a rectangular support polygon, each of the four boundaries is treated as a candidate tipping edge. The signed moment about edge e is calculated with Eq. (26): vertical weights contribute their perpendicular lever arms d_i,e, while horizontal wind, inertial and slope-equivalent forces contribute through their effective heights h_j,e. A positive value means that the resultant remains inside that edge; a zero value is incipient loss of compression; and a negative value indicates that the assumed rigid support cannot sustain static equilibrium without hold-down force.

$$\boldsymbol{r}_G = \frac{\sum_i m_i \boldsymbol{r}_i}{\sum_i m_i} \tag{25}$$

$$M_e = \sum_i W_i d_{i,e} - \sum_j F_j h_{j,e} \tag{26}$$

Equation (27) defines the dimensionless stability index used throughout the results. Normalisation by total vertical weight and the smaller support half-dimension makes results comparable across payload cases. The support set in Eq. (28) uses a = 0.565 m in both modes, b = 0.495 m for wheel-supported travel and b = 0.802 m for outrigger-supported lifting. Because the outriggers change only b, longitudinal lifts can remain critical even when the outriggers are fully deployed. This geometrical consequence is a central result rather than a numerical artefact.

$$SI = \frac{\min_e(M_e)}{W_{\text{tot}} \min(a,b)} \tag{27}$$

$$\mathscr{S} = \{(x,y) : -a \le x \le a,\ -b \le y \le b\} \tag{28}$$

Wind pressure was calculated using Eq. (29), with sea-level air density 1.225 kg m−3. The boom and payload wind forces were applied at effective heights of 1.50 m; the combined slewing/luffing inertial force was applied at 1.00 m. The slope contribution was represented by the downslope component of total weight acting at an effective height of 0.80 m. Complete three-dimensional force-application coordinates were unavailable, so these heights are documented modelling assumptions and are included in the sensitivity and limitation discussion.

$$p = \frac{1}{2}\rho_{\mathrm{air}} V^2 \tag{29}$$

Scenario matrix, uncertainty propagation and reproducibility

Deterministic sweeps covered boom azimuth from 0° to 360°, outward slope from 0° to 8.5°, wind speed from 0 to 20 m s−1 and central deck mass from 0 to 1500 kg. The four rated payload–reach pairs were evaluated directly. A separate load–radius envelope varied payload from 0 to 1000 kg and radius from 0.8 to 4.0 m; the boom centre-of-mass radius was approximated as 0.45r + 0.20 m for intermediate extensions. The envelope used the screening reserve SI ≥ 0.10, 1500 kg central deck mass, 3° slope, 15.5 m s−1 wind and deployed outriggers.

The uncertainty analysis used N = 10,000 independent evaluations per rated case and a fixed seed of 20260809. Deck mass was uniform from 800 to 1500 kg; slope was uniform from 0° to 8.5°; wind speed was a clipped normal distribution with mean 12 m s−1 and standard deviation 3 m s−1; azimuth was uniform from 0° to 360°; slewing acceleration was uniform from 0.10 to 0.60 m s−2; φ2 was uniform from 1.10 to 1.25; and fixed longitudinal centre-of-gravity error was normal with standard deviation 0.030 m. Equation (30) estimates the model-based probability of a negative stability index. This is a probability under the stated input distributions, not a fleet accident probability.

$$\widehat{P}_f = \frac{1}{N}\sum_{k=1}^{N} \mathbf{1}(SI_k < 0) \tag{30}$$

Results

Verification of load calculations

Using g = 9.81 m s−2, the four static payload weights are 1.962, 3.041, 4.415 and 7.848 kN. Applying φ2 = 1.202 increases them to 2.358, 3.655, 5.306 and 9.433 kN, respectively. The slewing/luffing forces increase from 80 N for the long-reach 200 kg case to 200 N for the short-reach 800 kg case, but their moments remain smaller than those created by payload weight at large radius. The calculation therefore identifies support-edge moment integration, rather than small rounding differences, as the decisive stability step.

The mass audit shows that a 500 kg unloaded vehicle would provide no credible static reserve for the long-reach configurations. The 1000 kg unloaded analysis mass is therefore decomposed into an 800 kg fixed remainder and a 200 kg moving boom. This definition makes the model reproducible while identifying a measurement priority: prototype weighing and corner-load measurements should replace the inferred component split before certification.

Table 7. Verified force values for the rated configurations using g = 9.81 m s⁻².

Case	Static payload force	Dynamic payload force	Slew/luff force	Rated reach

Case	Static payload force	Dynamic payload force	Slew/luff force	Rated reach
I	1.962 kN	2.358 kN	80 N	3.60 m
II	3.041 kN	3.655 kN	102 N	2.70 m
III	4.415 kN	5.306 kN	130 N	1.95 m
IV	7.848 kN	9.433 kN	200 N	1.13 m

Boom azimuth and support geometry

Figure 7 shows the minimum stability index for a 1000 kg central deck mass, a 3° outward slope and 15.5 m s−1 wind. The polar curves are strongly non-circular because the outrigger polygon is wider laterally than longitudinally. A side lift benefits from the 0.802 m lateral half-span, whereas a front or rear lift is limited by the unchanged 0.565 m longitudinal half-span. The small longitudinal offset of the fixed centre of gravity also breaks front–rear symmetry. Consequently, a single rated load–radius pair cannot describe stability over the full slew range.

Case I ranged from SI = -0.104 to 0.471; Case II from -0.133 to 0.450; Case III from -0.065 to 0.502; and Case IV from 0.111 to 0.627. Under this deliberately demanding combination, the two long-reach cases contained negative azimuth sectors even though the central deck mass was 1000 kg. Case IV remained positive over the entire rotation because its 800 kg payload was close to the slew centre. This result illustrates why payload mass alone is misleading: the 200 kg load produced a worse minimum margin than the 800 kg load because its horizontal radius was more than three times larger.

The model also distinguishes “non-negative” from “adequately reserved.” A state at SI = 0.01 satisfies the rigid-body sign criterion but offers little tolerance for support settlement, load sway, hydraulic compliance or centre-of-gravity error. The 0.10 screening line used for the load–radius envelope is therefore more informative for design iteration. It should not be treated as a substitute for a code-specific proof factor; rather, it defines a reproducible internal target while missing measurements are being acquired.

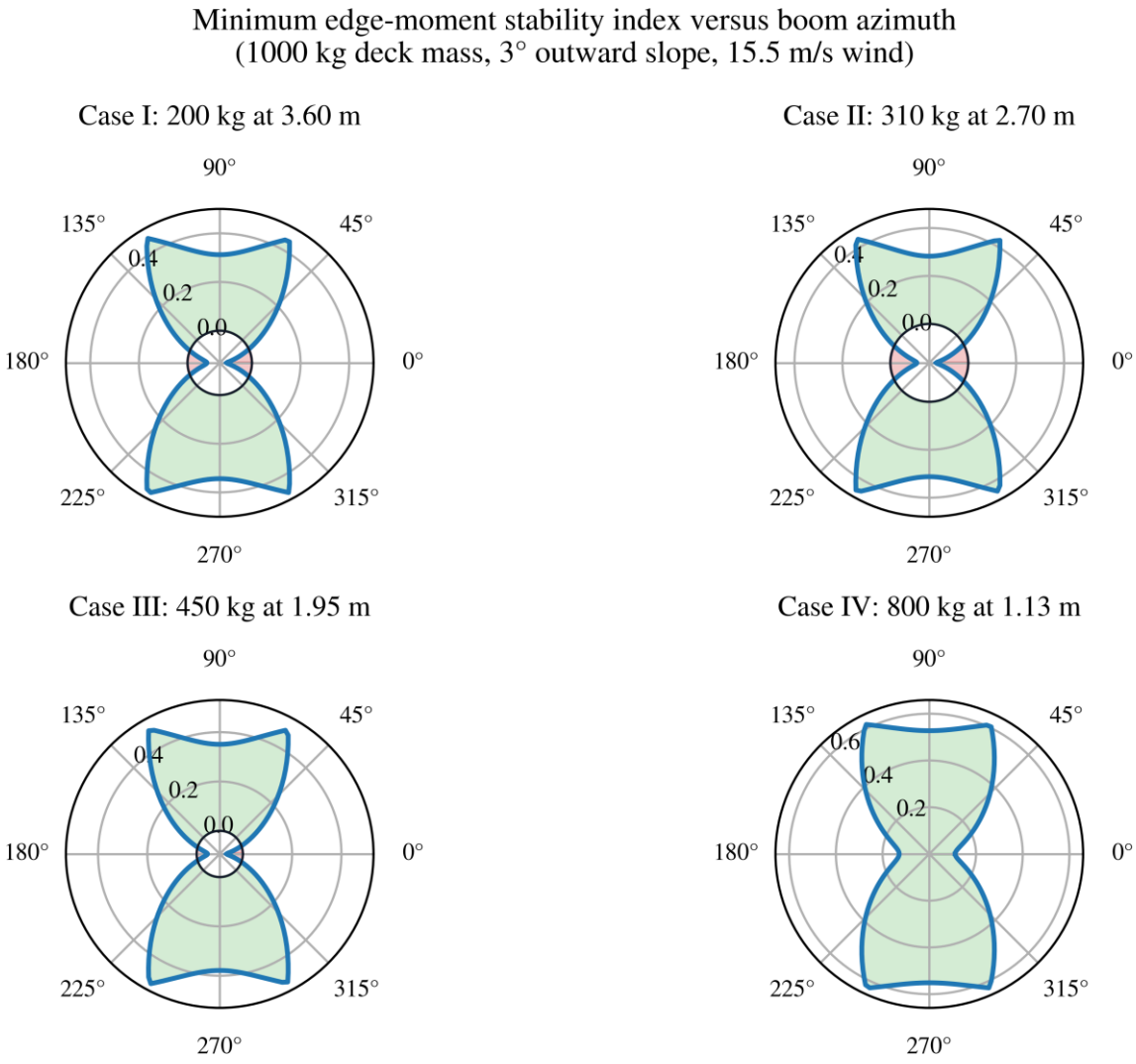


Figure 7. Computed minimum stability index versus boom azimuth for the four rated configurations. Green sectors are non-negative and red sectors are negative. The calculation assumes deployed outriggers, 1000 kg central deck mass, 3° outward slope and 15.5 m s^{-1} wind.

Coupled effects of slope and wind

Figure 8 evaluates a longitudinal lift with the maximum stated 1500 kg central deck mass. Longitudinal lifting was selected because the outriggers do not enlarge the 0.565 m longitudinal half-span and the sweep therefore exposes the slope–wind boundary that is hidden in a favourable side lift. The zero contour separates positive and negative edge moments. Increasing slope reduced stability more rapidly than increasing wind within the 0–20 m s−1 range because the downslope component of total weight acted on every mass, whereas the wind term acted only on the projected boom and payload areas. Nevertheless, wind shifted the boundary appreciably in the long-reach cases and should not be omitted from a site-specific decision.

Case I showed the smallest safe region. Its large payload radius and extended boom centre of mass placed substantial vertical moment outside the side support line. Case II was only moderately better because the additional payload partly offset the shorter reach. Case III had a wider admissible region, and Case IV had the largest positive reserve. These trends agree with the moment-arm structure of Eq. (26) and with recent wind-overturning studies in which crane orientation and geometry change the critical wind condition [9].

The heatmaps should be read as screening surfaces rather than weather limits. The assumed effective force heights, rigid ground, constant drag coefficient and wind direction aligned with the outward tipping direction are conservative simplifications. A real suspended payload can sway and generate transient moments not represented by a steady pressure. Conversely, sheltered sites or a wind direction that is not aligned with the

governing edge may be less demanding. An anemometer interlock should therefore use a validated site- and configuration-specific limit rather than treating 15.5 m s−1 as a universal threshold.

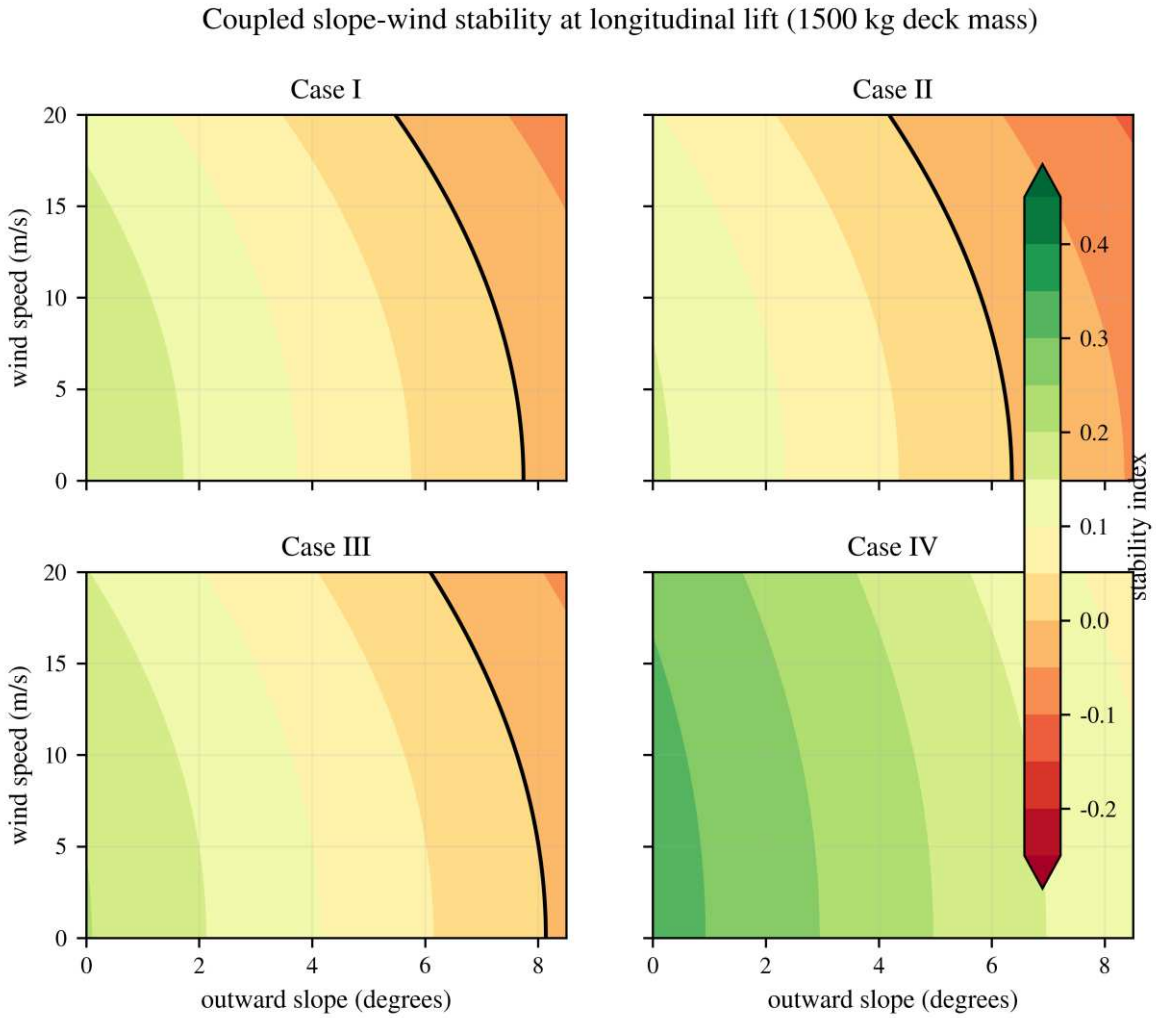


Figure 8. Model-derived slope–wind heatmaps for longitudinal lifting with 1500 kg central deck mass. The black contour denotes SI = 0; green regions are positive and red regions negative. These are computational screens, not certified weather limits.

Load–radius envelope and required deck mass

The continuous load–radius envelope in Fig. 9 translates the edge-moment calculation into a format familiar to lift planning. The curves show the maximum payload that maintained SI ≥ 0.10 under 3° slope, 15.5 m s−1 wind, 1500 kg central deck mass and deployed outriggers. Capacity decreased monotonically with radius, but the rate and absolute limit depended on azimuth. The 90° side-lift curve was most favourable because the lateral half-span was 0.802 m. The 0° longitudinal curve was most restrictive because the half-span remained 0.565 m. The 45° curve lay between them and was governed by whichever rectangular edge first lost moment reserve.

When the four rated operating points were superimposed, some approached or exceeded the SI ≥ 0.10 envelope for unfavourable azimuths. This does not prove that the vehicle will overturn, because the model does not include exact outrigger coordinates, distributed structural mass, tyre stiffness, ground compliance or a measured centre of gravity. It does show that a load table without azimuth and support-state qualifiers is under-specified. A practical rating chart should include at least payload, horizontal radius, slew sector, outrigger state, slope limit and wind limit.

Figure 10 expresses the same issue as the minimum central deck mass needed to avoid a negative edge moment. The maximum required masses over the full rotation were 1260, 1350, 1180 and 650 kg for Cases I–IV. Values above the 1500 kg carrying-mass limit cannot be achieved by simply retaining more deck cargo.

For those azimuths the design must instead shorten reach, reduce payload, enlarge the support polygon, add a dedicated counterweight within structural limits, or prohibit the lift. Because construction cargo is not a certified counterweight and may shift, relying on incidental deck material is not an acceptable final safety strategy.

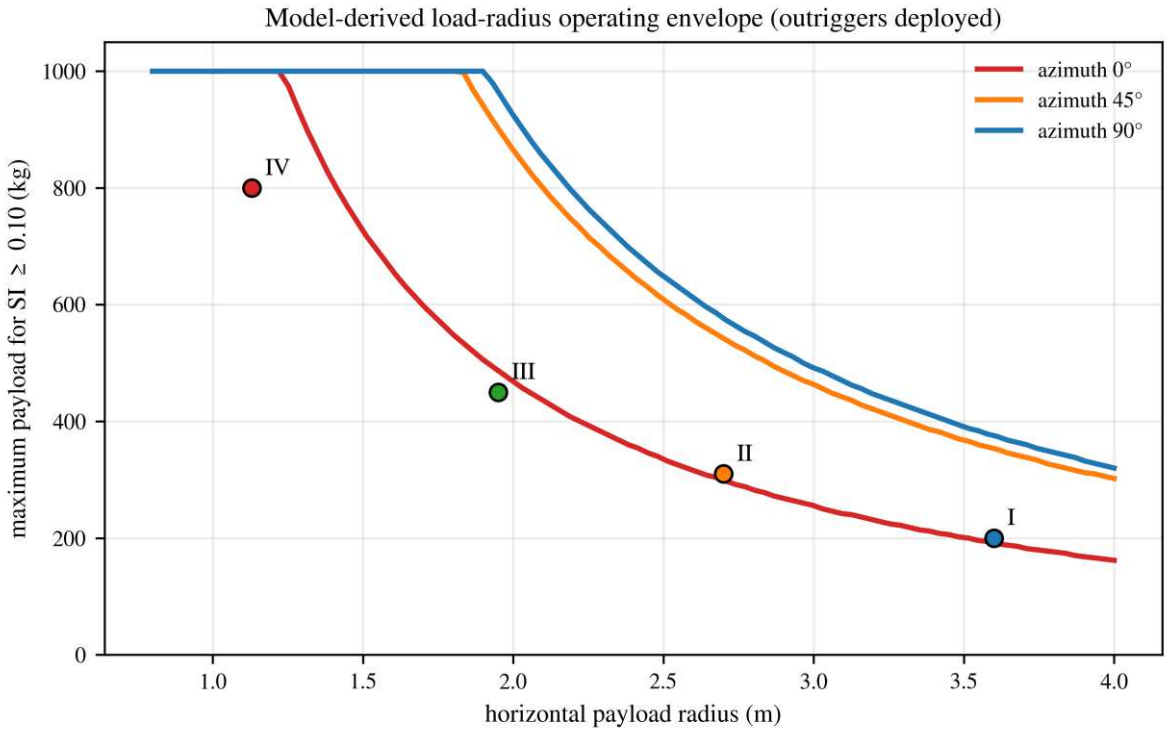


Figure 9. Computed load–radius envelope for a 0.10 stability-index reserve at three boom azimuths. The four markers denote the rated configurations. The envelope assumes deployed outriggers, 1500 kg central deck mass, 3° slope and 15.5 m s^{-1} wind.

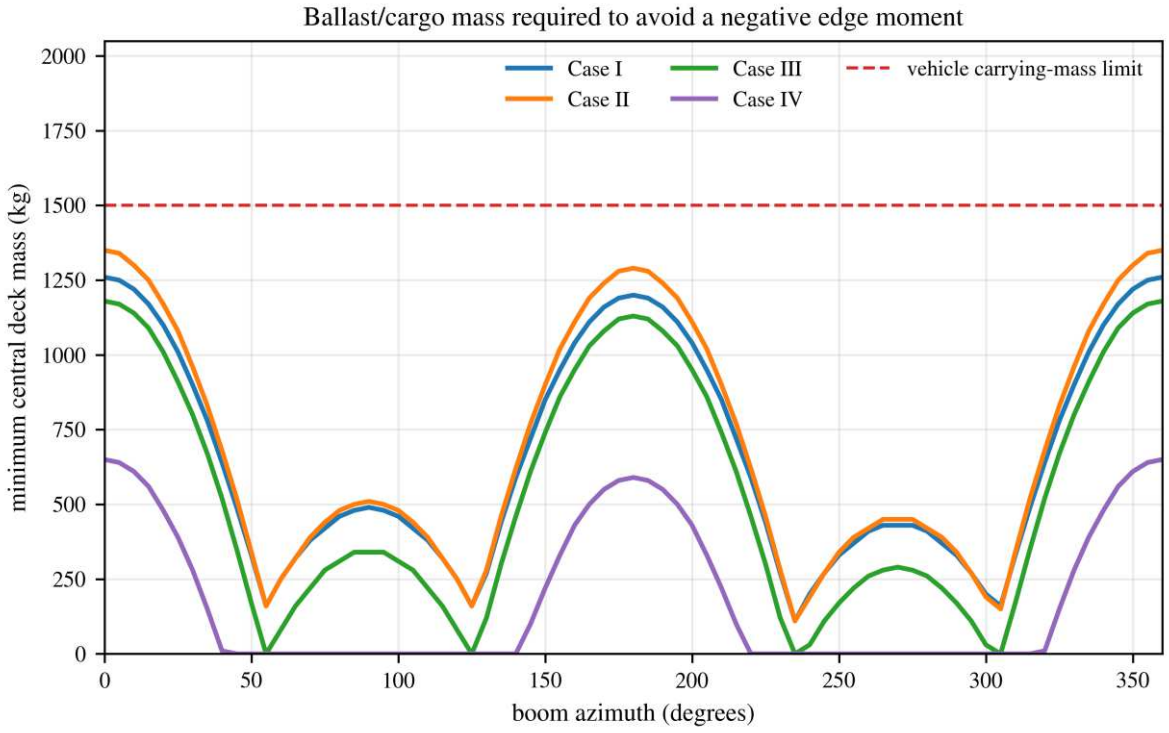


Figure 10. Central deck mass required to avoid a negative edge moment over the full boom rotation. The dashed line denotes the 1500 kg carrying-mass limit; deck cargo is analysed as a sensitivity variable and is not recommended as an unsecured counterweight.

Uncertainty propagation and sensitivity

The fixed-seed Monte Carlo results in Fig. 11 quantify how often the simplified model became negative under the stated input distributions. Median stability indices were 0.252, 0.226, 0.272 and 0.393 for Cases I–IV. The corresponding model-based negative-index probabilities were 16.1%, 20.8%, 13.0% and 0.8%. The distributions overlap substantially, showing that configuration ranking is conditional rather than absolute. A short-reach case can still become critical when the boom aligns with the narrow support dimension, deck mass is low and slope is high; conversely, an extended case can remain positive in a favourable side-lift sector with sufficient support reserve.

The fifth-to-ninety-fifth percentile intervals were [-0.116, 0.543], [-0.146, 0.514], [-0.082, 0.555] and [0.079, 0.667]. These broad intervals are a consequence of intentionally wide uncertainty ranges. They should not be interpreted as measurement confidence intervals. Their purpose is to test whether the design conclusion survives plausible variation in operating and geometric inputs. The result is clear: a pass/fail conclusion based on a single nominal orientation would not be robust.

Rank-correlation screening for Case I is shown in Fig. 12. Deck mass correlated positively with stability, while slope and the azimuth-dependent moment projection were the largest negative or non-monotonic contributors. Lifting coefficient, slewing acceleration, wind and centre-of-gravity error had smaller but non-zero effects within the selected ranges. Because azimuth is periodic, a simple rank correlation understates its structured influence; the polar sweep remains the appropriate diagnostic for that variable. The sensitivity analysis nevertheless identifies immediate measurement priorities: actual support geometry, total and component masses, centre-of-gravity coordinates, deck-load state and site slope should be known before refining less influential aerodynamic parameters.

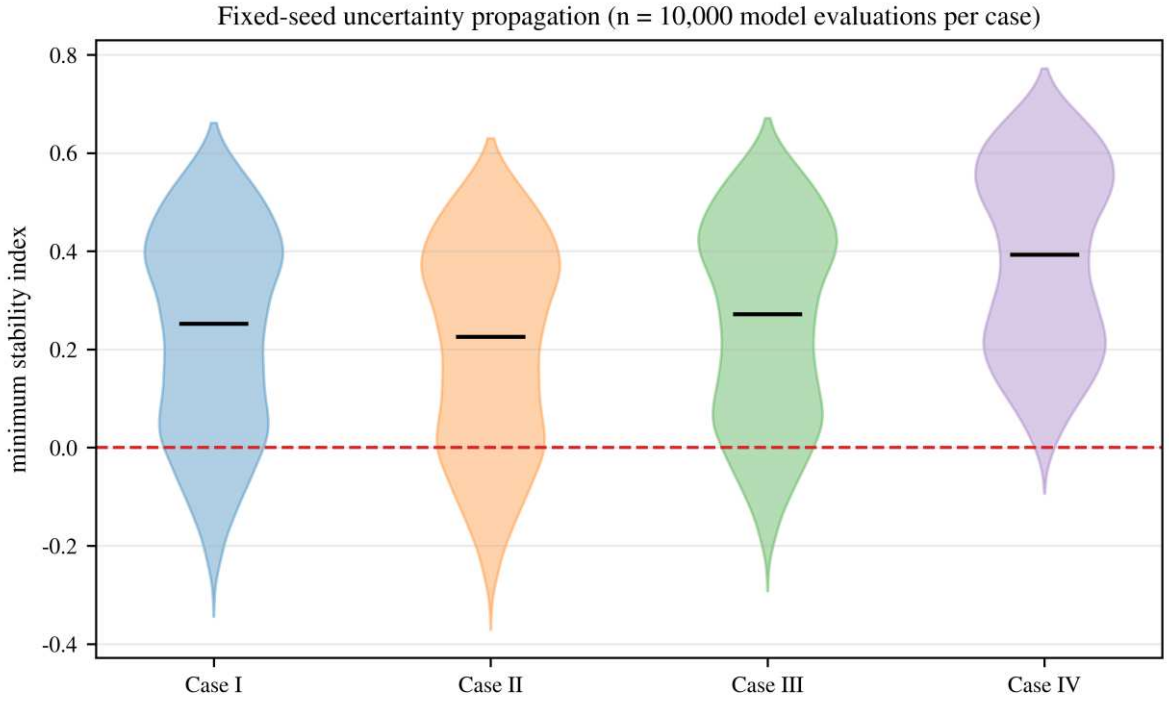


Figure 11. Fixed-seed Monte Carlo distributions of the model-derived minimum stability index (10,000 evaluations per rated case). The dashed line denotes incipient loss of edge-moment reserve. The probabilities apply only to the stated input distributions.

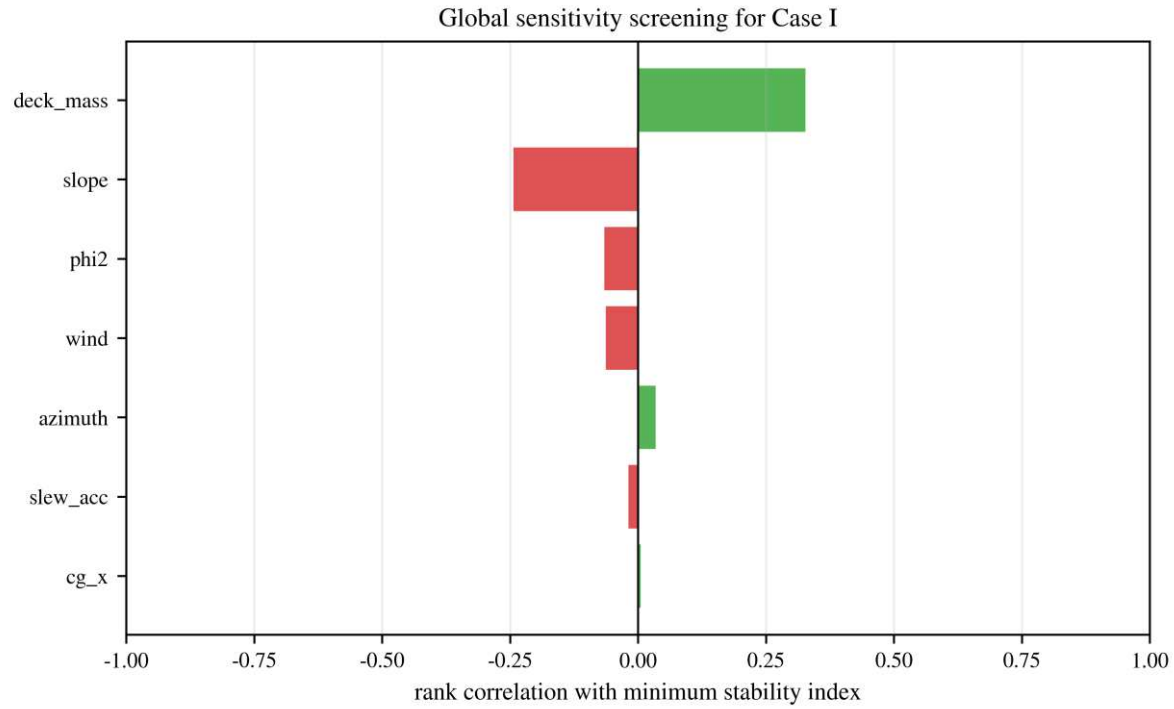


Figure 12. Rank-correlation sensitivity screening for the long-reach 200 kg configuration. Positive values increase the minimum stability index; negative values reduce it. Azimuth is periodic and is interpreted together with Fig. 7.

Table 8. Fixed-seed model uncertainty results (10,000 evaluations per case).

Rated case	Median SI	5th–95th percentile	Model P(SI < 0)
I	0.252	-0.116 to 0.543	16.1%
II	0.226	-0.146 to 0.514	20.8%
III	0.272	-0.082 to 0.555	13.0%
IV	0.393	0.079 to 0.667	0.8%

Discussion

From a normative load list to a testable stability claim

The main methodological contribution is the connection of a complete load model to a signed support-edge outcome. Every assumption is explicit: component mass, boom centre-of-mass radius, payload radius, support half-spans, force heights, slope, wind and acceleration. This transparency makes the calculation auditable and more useful for field measurement planning than a more detailed model whose parameters cannot be verified at the site.

The findings support the modern view that mobile-crane and mobile-manipulator stability is configuration dependent [1,3–5]. The support polygon determines which edge is critical, and the boom posture determines how much vertical and horizontal moment reaches that edge. Analytical support-force methods emphasise the same physical boundary: a tipping event begins when a support reaction approaches zero [4]. Our edge-moment index is a reduced-order representation of that condition. It is suitable for early design screening because it is inexpensive enough to evaluate thousands of states, yet it preserves the key geometry that a single global safety factor would hide.

A second contribution is the explicit separation of travel and lifting. Travel should occur with the boom stowed and outriggers retracted, whereas lifting should occur only after stopping, deploying supports and

verifying level. The load-combination table therefore applies only physically compatible actions to each scenario, preventing an unrealistically severe or physically impossible combination from being mistaken for an operational requirement.

Engineering implications

The first design implication is that the present outrigger concept enlarges only the lateral support dimension. That is effective for side lifts but does not protect front or rear lifts to the same degree. A mechanically simple improvement would be to reposition or redesign the outriggers so that the convex support polygon expands longitudinally as well as laterally. If geometry cannot be changed, the control system should implement slew-sector restrictions: long-reach lifts would be permitted only in validated side sectors, and the admissible sector would shrink with slope, wind or reduced deck/counterweight mass.

The second implication is that the four rated payloads should be expressed as a multidimensional chart rather than four isolated numbers. Figure 9 shows how capacity depends on radius and azimuth even before ground compliance is considered. A practical electronic load-moment limiter could use measured boom length, boom angle, slew angle, payload estimate, outrigger deployment and chassis inclination to query a validated envelope. The approach is compatible with recent dynamic tip-over-avoidance and mobile-manipulator stabilisation research [16,17], but it does not assume that software can compensate for an inadequate support polygon. Control should prevent entry into a hazardous state, not normalise operation at the tipping boundary.

The third implication concerns levelling and ground support. Synchronous platform-level control can reduce attitude error [8], but it cannot create bearing capacity. Each outrigger reaction must be transmitted through pads to soil or a prepared platform without excessive differential settlement. Soil stiffness and pad dimensions are outside the numerical model. In field deployment, a positive rigid-body moment must therefore be supplemented by a ground-bearing check and verification that all supports remain in contact. Road-level identification methods [7] and measured corner loads can provide the required state information.

The fourth implication is operational wind management. A single pressure cannot cover every configuration. Recent analytical wind-overturning studies show strong orientation dependence [9], and decision-support work treats wind as an input to crane selection rather than a generic afterthought [2]. The carrier should use an anemometer located away from local flow obstruction, a time-averaging rule and a gust criterion. The limit should be lower when a large-area payload is suspended or when the boom points toward the governing support edge. If measured wind exceeds the validated threshold, the load should be lowered and the boom returned to a stowed, low-area configuration.

The fifth implication is that incidental cargo should not be credited as permanent counterweight without restraint and verification. Figures 7 and 10 use central deck mass to show the strength of the mass effect, not to recommend carrying loose material during a lift. Cargo can shift, be removed without updating the load chart or exceed local structural capacity. A dedicated counterweight, if adopted, requires structural design, positive attachment, position sensing and inclusion in the certified mass properties. Otherwise the safe envelope must assume the minimum credible deck mass.

Safety management and the scope of mechanical modelling

Mechanical stability is only one layer of crane safety. Recent decision-support research identifies planning, supervision and human factors as interacting contributors [19]. Evolutionary-game analysis of tower-crane supervision shows that organisational incentives can affect compliance [20], while Bayesian-network analysis demonstrates coupling among human, machine, management and environmental risk factors [21]. Scenario-based accident assessment likewise argues for integrated rather than single-cause reasoning [22]. These studies concern larger construction cranes, but their systems lesson is directly relevant: a correct load chart is necessary and insufficient.

For the compact carrier, engineering controls should be paired with an operating procedure. Before lifting, the operator should verify that the vehicle is stationary, brakes are applied, outriggers are fully deployed, support pads are placed on adequate ground, chassis inclination is within the validated range, boom and payload inputs are correctly identified, and wind is below the configuration-specific limit. During lifting, an interlock

should prevent travel, detect loss of support pressure and stop motion before SI reaches the warning threshold. After an alarm, the safe response should prioritise lowering or retracting the load without slewing through a more hazardous sector.

Accident literature cautions against unsupported numerical effectiveness claims. A fatal overhead-crane forensic study illustrates the importance of reconstructing the actual sequence and physical evidence [23]. The present calculations therefore do not estimate a percentage reduction in accidents. Their defensible contribution is to identify stability-critical configurations and define variables that can be measured during prototype validation.

Limitations and validation plan

The most important limitation is the absence of hardware validation. The model assumes rigid bodies, a rectangular support polygon, no tyre or outrigger compliance, no structural deformation, no hydraulic drift and no suspended-load pendulum motion. Force-application heights are engineering assumptions, and the centre-of-gravity decomposition is inferred rather than measured with scales. Wind is represented as a steady resultant aligned with the outward tipping direction. Ground bearing, local pad settlement and soil–support interaction are not included. The Monte Carlo distributions represent epistemic and operational ranges selected for screening, not statistically fitted site populations.

These limitations define a concrete validation programme. First, weigh the complete unloaded machine and measure four wheel reactions on a level surface; repeat with the boom at selected lengths and azimuths to identify the moving mass and centre-of-gravity trajectory. Second, measure outrigger coordinates and reactions, including structural deflection, using load cells or calibrated pressure sensors. Third, perform slow static tilt-table or controlled platform-inclination tests without personnel in the hazard zone, stopping before support reaction reaches zero. Fourth, conduct instrumented lifting tests at the four rated configurations with increasing radius and multiple slew angles. Fifth, introduce controlled low-amplitude boom acceleration and record inertial response, load sway and support reaction. Finally, compare measured edge reactions and incipient lift-off states with model predictions and update the operating envelope using conservative residuals.

Validation should distinguish model calibration from independent testing. Component masses, centre-of-gravity coordinates and effective force heights may be estimated from a calibration subset. The calibrated parameters should then predict withheld configurations, slopes and payloads. Reporting only fitted cases would overstate accuracy. Positioning accuracy, road-level estimation and support-force sensing methods in recent crane and mobile-manipulator studies provide suitable measurement concepts [6–8]. Recent controlled tractor rollover experiments also illustrate the value of measuring complete reaction and inclination histories rather than only a terminal angle [25]. If discrepancies are large, a multibody or finite-element model may be warranted, especially to capture chassis torsion, which can alter rollover threshold [13].

The load equations follow GB/T 3811-2008 [24], but final conformity may require additional product-specific, vehicle, machinery-safety and local regulatory provisions. This article does not certify the design or replace a competent engineering review. The normative standard is older than the five-year research-literature window because it defines the governing load framework; the other 24 references are from 2021–2026 and provide the current research context.

Table 9. Proposed prototype-validation sequence derived from the model sensitivity and evidence gaps.

Priority	Required evidence	Purpose	Proposed acceptance output
1	Total mass and four-corner reactions	Resolve the 500/1000 kg inconsistency	Measured mass and CoG with uncertainty
2	Outrigger coordinates and reaction sensors	Validate support polygon and edge moment	Reaction residuals and lift-off threshold
3	Controlled slope tests	Validate gravity projection	Predicted versus measured critical angle
4	Instrumented rated lifts at multiple azimuths	Validate the load–radius envelope	Error-bounded sector load chart
5	Wind and dynamic-response testing	Calibrate force heights and transient factors	Validated interlock thresholds

Conclusions

This study presents a reproducible parametric stability assessment for a compact transmission-line construction carrier equipped with a crane boom. Twenty-four load equations, eight engineering figures and six parameter tables define a unified support-edge formulation for wheel-supported travel and outrigger-supported lifting. Consistent mass definitions, SI units and physically compatible load combinations make the analysis traceable and computationally reproducible.

The model-derived results demonstrate that stability is governed by the interaction of reach, azimuth, support geometry, slope, wind and available central mass. The 200 kg long-reach configuration can be less stable than the 800 kg short-reach configuration. Lateral outriggers improve side lifting but leave longitudinal sectors constrained by the 1.130 m support length. Under demanding model conditions, some rated configurations produce negative edge moments even with substantial central deck mass, so the four payload ratings should not be used without slew-sector, slope, wind and support-state qualifiers.

The results are screening calculations, not field measurements or certification evidence. Their value is that they expose the controlling assumptions, provide a load–radius–azimuth envelope and prioritise validation measurements. Before deployment, the complete machine mass, centre of gravity, outrigger reactions, ground bearing, dynamic response and wind limits must be measured and incorporated into a verified load-moment limiter and operating procedure.

Author contributions

Y.D. and F.Z. conceived the engineering problem. Y.D., F.Z. and Y.W. compiled vehicle and crane parameters. H.C. and Y.W. reviewed construction and cost constraints. All authors reviewed the analytical framework and approved the manuscript. The final contribution statement should be confirmed by all authors before submission.

Funding

This work was supported by the State Grid Jiangsu Electric Power Co., Ltd. science and technology project “Development of an autonomous material transport and loading vehicle for transmission-line construction” (HYS22Z10040).

Competing interests

The authors declare no competing interests. This statement should be reconfirmed before submission.

Data availability

All data generated or analysed during this study are included in this published article.

References

1. Kwiatoń, P., Cekus, D. & Waryś, P. Computer-aided rotary crane stability assessment. Automation in Construction 162, 105370 (2024). https://doi.org/10.1016/j.autcon.2024.105370
2. Hebiba, A. M., Bouferguene, A., Moon, S. & Han, S. Wind-wise automated stability analysis for selection of tower crane and location. Journal of Construction Engineering and Management 148, 04022127 (2022). https://doi.org/10.1061/(ASCE)CO.1943-7862.0002377
3. Song, J. & Sharf, I. Stability-constrained mobile manipulation planning on rough terrain. Robotica 40, 4090–4119 (2022). https://doi.org/10.1017/S0263574722000777
4. Petrović, G. R. & Mattila, J. Analytic solutions for wheeled mobile manipulator supporting forces. IEEE Access 10, 43235–43255 (2022). https://doi.org/10.1109/ACCESS.2022.3169766
5. Song, T., Yang, H., Guo, S. & Mohamed, R. P. Configuration selection for tip-over stability of a modular reconfigurable mobile manipulator under various application situations. Robotica 41, 1066–1085 (2023).
6. Kacalak, W., Budniak, Z. & Majewski, M. Modelling and analysis of the positioning accuracy in the loading systems of mobile cranes. Materials 15, 8426 (2022). https://doi.org/10.3390/ma15238426
7. Wang, G., Qu, W. & Chen, C. A road level identification method for all-terrain crane based on support vector machine. Measurement 187, 110319 (2022). https://doi.org/10.1016/j.measurement.2021.110319
8. Xu, F., Hu, H., Feng, S. & Zhou, C. Synchronous leveling control method of crane vehicle platform based on position–force coordination. Actuators 14, 441 (2025). https://doi.org/10.3390/act14090441
9. Augustyn, M. & Barski, M. Numerical and analytical determination of the critical wind speed causing the overturning of the top-slewing tower crane. Applied Sciences 15, 4683 (2025). https://doi.org/10.3390/app15094683
10. Cekus, D. & Kwiatoń, P. Stability analysis of mobile crane during wind-induced load sway. In: Advances in Mechanism and Machine Science, 2024, 147–158. https://doi.org/10.1007/978-3-031-56492-5_11
11. Jang, D.-H., Roh, G.-T., Jeon, C.-H. & Shim, C.-S. Simulation-based optimization of crane lifting position and capacity using a construction digital twin for prefabricated bridge deck assembly. Buildings 15, 475 (2025). https://doi.org/10.3390/buildings15030475
12. Wang, L. et al. Advances in tractor rollover and stability control: implications for off-road driving safety. Computers and Electronics in Agriculture 226, 109483 (2024). https://doi.org/10.1016/j.compag.2024.109483
13. Belloni, M., Vignati, M. & Sabbioni, E. Analysing the effect of chassis torsional flexibility on the rollover threshold of a multi-purpose agricultural vehicle. Vehicles 6, 415–432 (2024). https://doi.org/10.3390/vehicles6010018
14. Nguyen, T. A. Assessing the dependence of vehicle rollover on many factors based on new 4D graphs. PLoS ONE 18, e0284018 (2023). https://doi.org/10.1371/journal.pone.0284018
15. Sun, L., Chen, L., Yin, Y., Tian, Y. & Zhang, X. Risk assessment of rollover and skidding due to pavement roughness and differential settlement for enhancing transportation safety. Journal of Advanced Transportation 2021, 7244283 (2021). https://doi.org/10.1155/2021/7244283
16. Tao, Y., Liu, H., Song, Y., Deng, C., Wang, B. & Zheng, P. Dynamic tip-over avoidance method for mobile manipulators based on the extended zero-moment point algorithm for human–robot collaboration. Journal of Computing and Information Science in Engineering 25, 051003 (2025). https://doi.org/10.1115/1.4067523
17. Toledo Fuentes, A., Kempf, F., Kipfmüller, M., Bergmann, T. & Prieto, M. J. Tip-over detection and avoidance algorithms as stabilization strategy for small-footprint and lightweight mobile manipulators. Machines 11, 44 (2023). https://doi.org/10.3390/machines11010044
18. Chuang, C., Zhang, H., Peng, H. & Lu, H. Stability control for end effector of mobile manipulator in uneven terrain based on active disturbance rejection control. Assembly Automation 41, 2021. https://doi.org/10.1108/AA-10-2020-0157
19. Sadeghi, H. & Zhang, X. Towards safer tower crane operations: an innovative knowledge-based decision support system for automated safety risk assessment. Journal of Safety Research 90, 272–294 (2024). https://doi.org/10.1016/j.jsr.2024.05.011
20. Chen, Y., Zeng, Q., Zheng, X., Shao, B. & Jin, L. Safety supervision of tower crane operation on construction sites: an evolutionary game analysis. Safety Science 152, 105578 (2022). https://doi.org/10.1016/j.ssci.2021.105578
21. Wu, B.-J., Jin, L.-H., Zheng, X.-Z. & Chen, S. Coupling analysis of crane accident risks based on Bayesian network and the N-K model. Scientific Reports 14, 1133 (2024). https://doi.org/10.1038/s41598-024-51425-9
22. He, W., Lin, Z., Li, W., Wong, C. J., Kong, D. & Loh, W. E. The comprehensive safety assessment method for complex construction crane accidents based on scenario analysis: a case study of crane accidents. Computers & Industrial Engineering 199, 110716 (2025). https://doi.org/10.1016/j.cie.2024.110716
23. Ziernicki, R. & Nguyen, R. Forensic engineering analysis of fatal overhead crane accident. Journal of the National Academy of Forensic Engineers 37, 1 (2021). https://doi.org/10.51501/jotnafe.v37i1.114
24. GB/T 3811-2008. Design Rules for Cranes. Standardization Administration of China, Beijing (2008).
25. Carabin, G., Karaca, M. & Mazzetto, F. Preliminary results of extensive tractor rollover stability tests using a tilting-rotating rig. Biosystems Engineering 254, 104146 (2025). https://doi.org/10.1016/j.biosystemseng.2025.104146